

# Tension and Systematics in the Gold06 SnIa Dataset

S. Nesseris<sup>a</sup> and L. Perivolaropoulos<sup>b</sup>

*Department of Physics, University of Ioannina, Greece*

<sup>a</sup> e-mail: me01629@cc.uoi.gr, <sup>b</sup> e-mail: leandros@uoi.gr

(Dated: February 7, 2020)

The Gold06 SnIa dataset recently released in astro-ph/0611572 consists of five distinct subsets defined by the group or instrument that discovered and analyzed the corresponding data. These subsets are: the SNLS subset (47 SnIa), the HST subset (30 SnIa), the HZSST subset (41 SnIa), the SCP subset (26 SnIa) and the Low Redshift (LR) subset (38 SnIa). These subsets sum up to the 182 SnIa of the Gold06 dataset. We use Monte-Carlo simulations to study the statistical consistency of each one of the above subsets with the full Gold06 dataset. In particular, we compare the best fit  $w(z)$  parameters ( $w_0, w_1$ ) obtained by subtracting each one of the above subsets from the Gold06 dataset (subset truncation), with the corresponding best fit parameters ( $w_0^r, w_1^r$ ) obtained by subtracting the same number of *randomly selected* SnIa from the same redshift range of the Gold06 dataset (random truncation). We find that the probability for  $(w_0^r, w_1^r) = (w_0, w_1)$  is large for the Gold06 minus SCP (Gold06-SCP) truncation but is less than 5% for the Gold06-SNLS, Gold06-HZSST and Gold06-HST truncations. This result implies that the Gold06 dataset is not statistically homogeneous. By comparing the values of the best fit  $(w_0, w_1)$  for each subset truncation we find that the tension among subsets is such that the SNLS and HST subsets are statistically consistent with each other and ‘pull’ towards  $\Lambda$ CDM ( $w_0 = -1, w_1 = 0$ ) while the HZSST subset is statistically distinct and strongly ‘pulls’ towards a varying  $w(z)$  crossing the line  $w = -1$  from below ( $w_0 < -1, w_1 > 0$ ). We also isolate six SnIa that are mostly responsible for this behavior of the HZSST subset.

PACS numbers: 98.80.Es, 98.65.Dx, 98.62.Sb

## I. INTRODUCTION

Current cosmological observations show strong evidence that we live in a spatially flat universe [1] with low matter density [2] that is currently undergoing accelerated cosmic expansion. The most direct indication for the current accelerating expansion comes from the accumulating type Ia supernovae (SnIa) data [3, 4, 5, 6, 7, 8, 9] which provide a detailed form of the recent expansion history of the universe.

This accelerating expansion has been attributed to a dark energy component with negative pressure which can induce repulsive gravity and thus cause accelerated expansion (for recent reviews see [10, 11, 12, 13, 14, 15, 16]) The simplest and most obvious candidate for this dark energy is the cosmological constant  $\Lambda$  [17] with equation of state  $w = p/\rho = -1$ . This model however raises theoretical problems related to the fine tuned value required for the cosmological constant. These difficulties have lead to a large variety of proposed models where the dark energy component evolves with time usually due to an evolving scalar field (quintessence) which may be minimally [18] or non-minimally [19] coupled to gravity. Alternatively, more general modified gravity theories[20] have also been proposed based on  $f(R)$  theories[21, 22, 23, 24], braneworlds[25, 26, 27, 28], Gauss-Bonnet dark energy[29] etc. The main prediction of the dynamical models is the evolution of the dark energy density parameter  $\Omega_X(z)$ . Combining this prediction with the prior assumption for the matter density parameter  $\Omega_{0m}$ , the predicted expansion history  $H(z)$  is

obtained as

$$H(z)^2 = H_0^2[\Omega_{0m}(1+z)^3 + \Omega_X(z)] \quad (1.1)$$

The dark energy density parameter is usually expressed as

$$\Omega_X(z) = \Omega_{0X} e^{3 \int_0^z \frac{dz'}{1+z'}(1+w(z'))} \quad (1.2)$$

where  $w(z)$  is related to  $H(z)$  by [30, 31, 32]

$$w(z) = \frac{\frac{2}{3}(1+z)\frac{d\ln H}{dz} - 1}{1 - (\frac{H_0}{H})^2\Omega_{0m}(1+z)^3} \quad (1.3)$$

If the dark energy can be described as an ideal fluid with conserved energy momentum tensor  $T^{\mu\nu} = \text{diag}(\rho, p, p, p)$  then the above parameter  $w(z)$  is identical with the equation of state parameter of dark energy

$$w(z) = \frac{p(z)}{\rho(z)} \quad (1.4)$$

Independently of its physical origin, the parameter  $w(z)$  is an observable derived from  $H(z)$  (with prior knowledge of  $\Omega_{0m}$ ) and is usually used to compare theoretical model predictions with observations.

The two most reliable and robust SnIa datasets existing at present are the Gold dataset [9] (hereafter Gold06) and the Supernova Legacy Survey (SNLS) [7] dataset. The Gold dataset compiled by Riess et. al. is a set of 182 supernova data from various sources analyzed in a consistent and robust manner with reduced calibration errors arising from systematics. It contains 119 points

from previously published data [8] (hereafter Gold04) plus 16 points with  $0.46 < z < 1.39$  discovered recently by the Hubble Space Telescope (HST). It also incorporates 47 points ( $0.25 < z < 1$ ) from the first year release of the SNLS dataset [7] out of a total of 73 distant SnIa. Some supernovae were excluded[9] due to highly uncertain color measurements, high extinction  $A_V > 0.5$  and a redshift cut  $cz < 7000 \text{ km/s}$  or  $z < 0.0233$ , to avoid the influence of a possible local “Hubble Bubble”, so as to define a high-confidence subsample. In addition, a single algorithm (MLCS2k2) was applied to estimate all the SnIa distances (including those originating from SNLS) thus attempting to minimize the non-uniformities of the dataset.

The total of 182 SnIa included in the Gold06 dataset can be grouped into five subsets according to the search teams/instruments that discovered them. These subsets are shown in Table I. A detailed table of all the data used in our analysis and their subset origin is shown in the Appendix. Notice that the early data of the Gold06 dataset were obtained mainly in the 90’s and consist of the High z Supernova Search Team (HZSST) subset, the Supernova Cosmology Project (SCP) subset and the Low Redshift (LR) subset.

The above observations provide the apparent magnitude  $m(z)$  of the supernovae at peak brightness after implementing correction for galactic extinction, K-correction and light curve width-luminosity correction. The resulting apparent magnitude  $m(z)$  is related to the luminosity distance  $d_L(z)$  through

$$m_{th}(z) = \bar{M}(M, H_0) + 5\log_{10}(D_L(z)) \quad (1.5)$$

where in a flat cosmological model

$$D_L(z) = (1+z) \int_0^z dz' \frac{H_0}{H(z'; a_1, \dots, a_n)} \quad (1.6)$$

is the Hubble free luminosity distance ( $H_0 d_L/c$ ),  $a_1, \dots, a_n$  are theoretical model parameters and  $\bar{M}$  is the magnitude zero point offset and depends on the absolute magnitude  $M$  and on the present Hubble parameter  $H_0$  as

$$\begin{aligned} \bar{M} &= M + 5\log_{10}\left(\frac{c H_0^{-1}}{\text{Mpc}}\right) + 25 = \\ &= M - 5\log_{10}h + 42.38 \end{aligned} \quad (1.7)$$

The parameter  $M$  is the absolute magnitude which is assumed to be constant after the above mentioned corrections have been implemented in  $m(z)$ .

The data points of the Gold06 dataset are given after the corrections have been implemented, in terms of the distance modulus

$$\mu_{obs}(z_i) \equiv m_{obs}(z_i) - M \quad (1.8)$$

The theoretical model parameters are determined by minimizing the quantity

$$\chi^2(a_1, \dots, a_n) = \sum_{i=1}^N \frac{(\mu_{obs}(z_i) - \mu_{th}(z_i))^2}{\sigma_{\mu_i}^2 + \sigma_{v_i}^2} \quad (1.9)$$

TABLE I: The subsets of the Gold06 dataset (see also [33]).

Subsets	Total	Redshift Range	Years of discovery	Ref.
SNLS	47	$0.25 \leq z \leq 0.96$	2003-2004	[7]
HST	30	$0.46 \leq z \leq 1.76$	1997-2005	[9]
HZSST	41	$0.28 \leq z \leq 1.20$	1995-2001	[3]
SCP	26	$0.17 \leq z \leq 0.86$	1995-2000	[4]
LR	38	$0.024 \leq z \leq 0.12$	1990-2000	[5]

where  $\sigma_{\mu_i}^2$  and  $\sigma_{v_i}^2$  are the errors due to flux uncertainties and peculiar velocity dispersion respectively. These errors are assumed to be gaussian and uncorrelated. The theoretical distance modulus is defined as

$$\mu_{th}(z_i) \equiv m_{th}(z_i) - M = 5\log_{10}(D_L(z)) + \mu_0 \quad (1.10)$$

where

$$\mu_0 = 42.38 - 5\log_{10}h \quad (1.11)$$

and  $\mu_{th}(z_i)$  also depends on the parameters  $a_1, \dots, a_n$  used in the parametrization of  $H(z)$  in equation (1.6).

The parametrization used in our analysis is the CPL parametrization [34, 35]

$$w(z) = w_0 + w_1 \frac{z}{1+z} \quad (1.12)$$

$$\begin{aligned} H^2(z) &= H_0^2 [\Omega_{0m}(1+z)^3 + \\ &+ (1-\Omega_{0m})(1+z)^{3(1+w_0+w_1)} e^{3w_1[1/(1+z)-1]}] \end{aligned} \quad (1.13)$$

with a prior of the matter density parameter  $\Omega_{0m} = 0.28$  (as in Ref. [9]), assuming flatness, according to the methods described in detail in Ref. [36, 37].

The previous version of the Gold sample [8] (Gold04) had been shown to be in mild ( $2\sigma$ ) tension with the SNLS dataset [37, 38]. While the Gold04 mildly favored an evolving dark energy equation of state parameter  $w(z)$  (crossing the phantom divide line  $w=-1$ ) over the cosmological constant ( $\Lambda$ CDM) at almost  $2\sigma$  level [36, 39, 40, 41, 42, 43], the SNLS data had shown no such trend and provided [37] a best fit  $w(z)$  very close to  $w = -1$  ( $\Lambda$ CDM). The trend towards phantom divide crossing can not be explained in the context of minimally coupled quintessence and could be viewed as an indication for more exotic models [44, 45, 46, 47, 48, 49, 50, 51]. This mild tension could have been attributed to systematic errors due eg to the different algorithm used in the analysis of the two datasets. The new version of the Gold sample however, (Gold06) involves an improved uniform analysis and incorporates a large part of the SNLS sample. Thus there could have been an anticipation that the mild tension with SNLS would be ameliorated or even disappear. As shown in Fig. 1 however, this anticipation has not been fulfilled (see also [52, 53]).

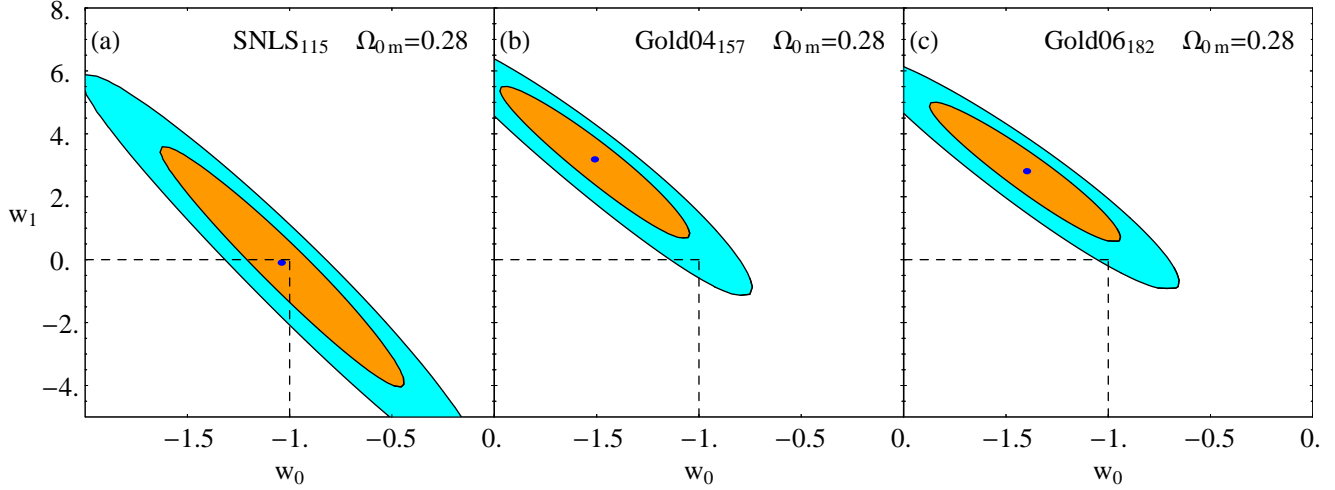


FIG. 1: Maximum likelihood fits of the CPL parametrization (1.12) to the SNLS (a) Gold04 (b) and Gold06 (c) datasets. The  $2\sigma$  tension between the Gold and SNLS remains with the new Gold06 dataset despite the improved filtering, calibration and data extension.

The mild (almost  $2\sigma$ ) tension between the Gold04 and the SNLS samples (Figs. 1a and 1b) has not decreased by using the Gold06 sample (Fig. 1c)! The investigation of the origin of this tension and the statistical uniformity of the Gold06 dataset consist the main focus of the present paper.

## II. TENSION IN THE GOLD06 DATASET

The 182 SNIa included in the Gold06 dataset originate mainly from the search teams/instruments shown in Table I. The low redshift subset (LR) is a mixture of various early SNIa by different groups and instruments but we consider it as a single subset because otherwise we would have to increase the number of subsets beyond a reasonable number.

In order to investigate the statistical uniformity of the Gold06 dataset and also the origin of the tension with the SNLS, we have decomposed the Gold06 dataset into the subsamples of Table I and constructed new datasets by subtracting each one (or two) of the subsets from the full Gold06 dataset. We thus obtained the following six subset truncations:

1.  $182_{G06} - 47_{SNLS} - 30_{HST}$
2.  $182_{G06} - 47_{SNLS}$
3.  $182_{G06} - 30_{HST}$
4.  $182_{G06} - 26_{SCP}$
5.  $182_{G06} - 41_{HZSST}$
6.  $182_{G06} - 41_{HZSST} - 26_{SCP}$

We did not consider the subset  $182_{G06} - 38_{LR}$  with low redshift truncation because the  $LR$  subset is not uniform and also because subtracting it can not be associated with a corresponding random truncation in the same low redshift range (the range  $z < 0.124$  is spanned completely by the  $LR$  subset). We then addressed the following two questions:

- How do the best fit  $(w_0, w_1)$  values for each of the six truncations compare with the corresponding best fit value of the full Gold06 dataset?
- How do the best fit  $(w_0, w_1)$  values for each of the six truncations compare with the corresponding best fit value of a random truncation of the full Gold06 dataset made in the same redshift range as that of the subtracted subset?

The answer to the first question is provided in Fig. 2 where we show the best fit values  $(w_0, w_1)$  for each one of the above six truncations. Notice that the two multiple truncations:  $182_{G06} - 41_{HZSST} - 26_{SCP}$  (point 1) and  $182_{G06} - 47_{SNLS} - 30_{HST}$  (point 6) correspond to more extreme best fit values of  $(w_0, w_1)$ . The best fit  $(w_0, w_1)$  of the Gold06 dataset along with its  $1\sigma$  and  $2\sigma$  contours is also shown in Fig. 2 (point 0).

The following comments can be made on the basis of Fig. 2:

- The truncation  $182_{G06} - 26_{SCP}$  leaves the best fit  $(w_0, w_1)$  of the Gold06 dataset practically unchanged
- No single subset truncation is able to shift the best fit  $(w_0, w_1)$  values beyond the  $1\sigma$  contours of the Gold06 dataset.

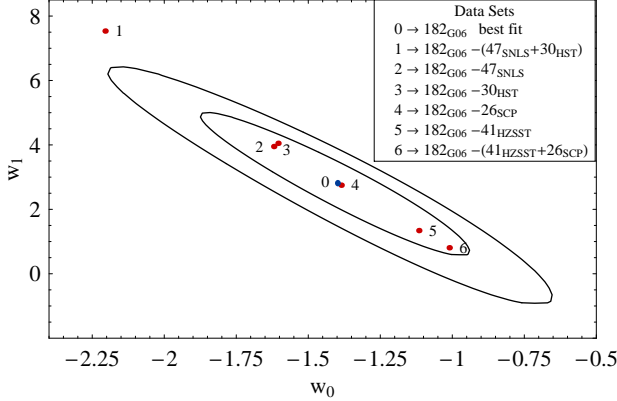


FIG. 2: The  $1\sigma$  –  $2\sigma$   $\chi^2$  confidence region ellipses in the  $w_0$  –  $w_1$  plane based on parametrization (1.12) for the Gold06 dataset and  $\Omega_{0m} = 0.28$ . Superposed are the best fit parameter values for each one of the truncations 1-6 of the Gold06 dataset.

- All the subset truncations (except  $182_{G06} - 26_{SCP}$ ) systematically shift the best fit  $(w_0, w_1)$  along the major axis of the  $\chi^2$  ellipse. In particular for  $182_{G06} - 30_{HST}$  and  $182_{G06} - 47_{SNLS}$  the best fit is left mainly under the influence of  $HZSST$  and is shifted along the major axis, away from  $\Lambda$ CDM towards an evolving  $w(z)$  crossing the line  $w = -1$  ( $w_0 < -1$ ,  $w_1 > 0$ ). On the other hand for  $182_{G06} - 41_{HZSST}$  the best fit  $(w_0, w_1)$  is left under the influence of  $HST$  and  $SNLS$  and is shifted towards  $\Lambda$ CDM. This implies that the subsets  $HST$  and  $SNLS$  favor  $\Lambda$ CDM while the subset  $HZSST$  favors an evolving  $w(z)$  crossing the phantom divide  $w = -1$ . This result is further amplified by the behavior of the multiple truncations  $182_{G06} - 41_{HZSST} - 26_{SCP}$  (further shifted towards  $\Lambda$ CDM) and  $182_{G06} - 47_{SNLS} - 30_{HST}$  (strongly shifted towards a varying  $w(z)$  crossing the phantom divide  $w = -1$  at a level more than  $2\sigma$  (see Fig. 2)).

Based on the above comments we conclude that the answer to the first question stated above can be summarized as follows: The best fit  $(w_0, w_1)$  values for each of the four single set truncations 2-5 do not differ more than  $1\sigma$  from the best fit corresponding values of the Gold06 dataset but they show distinct trends which are characteristic for each one of the truncations.

A separate question (related to the second question stated above) is the question of statistical consistency between each subset truncation and the full Gold06 dataset. To address this question we compare the best fit value of  $(w_0, w_1)$  for each subset truncation with a large number (500) of corresponding random truncations of the Gold06 dataset. The random truncations involve random subtractions of the same number of SNIa and in the same redshift range as the subset truncation. These random truncations can be used to obtain the  $1\sigma$  range for the

TABLE II: The six subset truncations of Fig 3.

Dataset	$w_0$	$w_1$	$\frac{w_0^r}{w_1^r}$ (MC)	$\frac{w - \bar{w}^r}{\sigma_{w^r}}$
$182 - 47_{SNLS} - 30_{HST}$	$w_0 = -2.21$	$w_1 = 7.53$	$\frac{w_0^r}{w_1^r} = -1.40 \pm 0.22$	$-3.7\sigma$
$182 - 47_{SNLS}$	$w_0 = -1.62$	$w_1 = 3.95$	$\frac{w_0^r}{w_1^r} = -1.38 \pm 0.12$	$-2.2\sigma$
$182 - 30_{HST}$	$w_0 = -1.60$	$w_1 = 4.05$	$\frac{w_0^r}{w_1^r} = -1.36 \pm 0.10$	$-2.4\sigma$
$182 - 26_{SCP}$	$w_0 = -1.39$	$w_1 = 2.75$	$\frac{w_0^r}{w_1^r} = -1.40 \pm 0.08$	$+0.2\sigma$
$182 - 41_{HZSST}$	$w_0 = -1.12$	$w_1 = 1.34$	$\frac{w_0^r}{w_1^r} = -1.40 \pm 0.11$	$+2.7\sigma$
$182 - 41_{HZSST} - 26_{SCP}$	$w_0 = -1.01$	$w_1 = 0.81$	$\frac{w_0^r}{w_1^r} = -1.39 \pm 0.15$	$+2.6\sigma$

expected values of the best fit  $(w_0^r, w_1^r)$  of the randomly truncated Gold06 dataset.

If the best fit values  $(w_0, w_1)$  of the subset truncation is within the  $1\sigma$  range of the best fit values  $(w_0^r, w_1^r)$  of the random truncation then the considered subset truncation is a typical truncation representative of the Gold06 dataset and statistically consistent with it. If on the other hand  $(w_0, w_1)$  differs by  $2\sigma$  or more from the mean best fit values  $(\bar{w}_0^r, \bar{w}_1^r)$  of the random truncation then the considered subset truncation is not a typical truncation and is systematically different from the full dataset. We have implemented the above comparison for the six subset truncations referred above and the results are shown in Table II and in Fig. 3.

The following comments can be made on the basis of Table II and Fig. 3:

- The  $SCP$  is a typical, statistically consistent subset of the Gold06 dataset because its truncation does not significantly alter the statistical properties of the Gold06 dataset. In particular the best fit  $(w_0, w_1)$  value of the  $182_{G06} - 26_{SCP}$  truncation differs only by  $0.2\sigma$  from the corresponding mean random truncation best fit  $(\bar{w}_0^r, \bar{w}_1^r)$  which involves random subtraction of the same number of SNIa from the same redshift range as the SCP subset.
- The other five subsets considered in Fig. 3 are not typical subsets of the Gold06 dataset. The best fit  $(w_0, w_1)$  values of the truncations considered in Fig. 3 differ by more than  $2\sigma$  from the mean best fit values  $(\bar{w}_0^r, \bar{w}_1^r)$  of the corresponding random truncations.
- An extreme case is the truncation  $182_{G06} - 47_{SNLS} - 30_{HST}$  whose best fit values are  $3.7\sigma$  away from the corresponding mean best fit values of a random truncation! This implies that the combination of the  $38_{LR} + 41_{HZSST} + 26_{SCP}$  which is left over from the truncation  $182_{G06} - 47_{SNLS} - 30_{HST}$

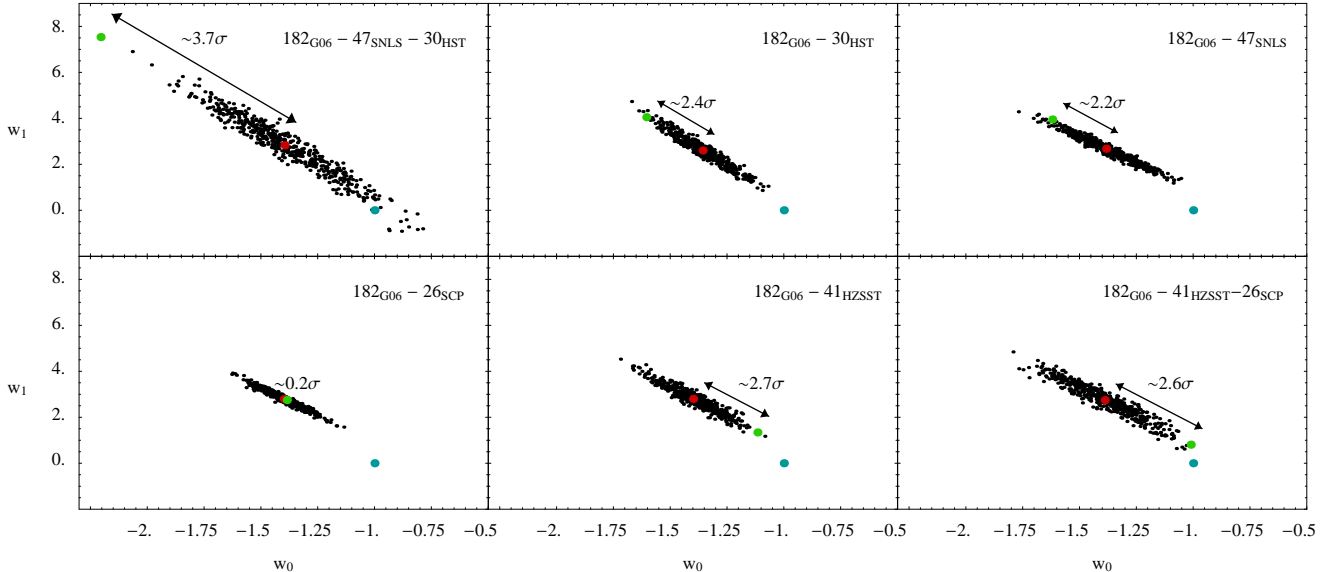


FIG. 3: Comparison of the best fit parameters to the subsample truncations 1-6 with corresponding random truncations of the Gold06 dataset. In all truncation cases (except of the SCP truncation) the best fit parameter values are shifted (in different directions) by more than  $2\sigma$  from the mean random truncation values. The point corresponding to  $\Lambda$ CDM ( $w_0 = -1, w_1 = 0$ ) is also shown.

strongly favors an evolving  $w(z)$  and is statistically inconsistent with the Gold06 dataset. This result is consistent with Fig. 2 which also shows that best fit ( $w_0, w_1$ ) of the truncation  $182_{G06} - 47_{SNLS} - 30_{HST}$  is about  $3\sigma$  away from the Gold06 best fit!

- The  $182_{G06} - 47_{SNLS}$  and  $182_{G06} - 30_{HST}$  are statistically very similar to each other (with a trend towards  $\Lambda$ CDM) even though they are both significantly different (more than  $2\sigma$ ) from the corresponding random truncations of Gold06 (see also Fig. 2).
- Both Figs 2 and 3 indicate that the trend towards  $\Lambda$ CDM increases for more recent ( $HST$  and  $SNLS$ ) data while earlier data ( $HZSST$  and  $SCP$ ) seem to favor and evolving  $w(z)$ .

The above results can also be verified by considering the ‘pure’ Gold06 dataset which does not include the 47 SnIa of SNLS. This dataset (Gold06p) consists of 135 SnIa and is essentially a filtered version of the Gold04 dataset with the addition of the 16 SnIa with  $0.46 < z < 1.39$  discovered recently by the HST. The best fit parameter values for the Gold06p dataset are somewhat shifted in the direction of varying  $w(z)$  compared to the full Gold06 (compare Figs. 2 and 4) as expected since SNLS favors  $\Lambda$ CDM. As shown in Fig. 4 and Table III, the effect of each subset truncation in this case is more prominent due to the smaller number of points in the Gold06p dataset.

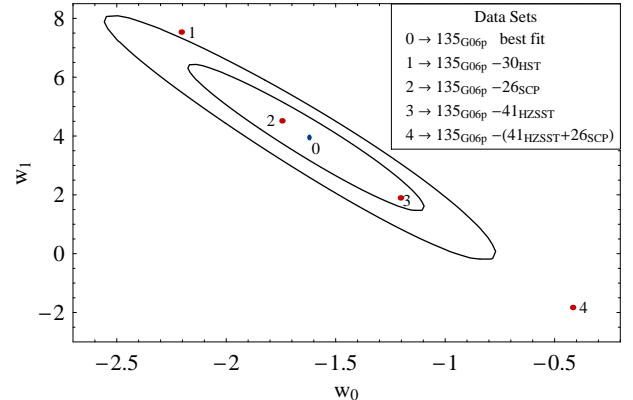


FIG. 4: The  $1\sigma - 2\sigma$   $\chi^2$  confidence region ellipses in the  $w_0 - w_1$  plane based on parametrization (1.12) for the Gold06p dataset and  $\Omega_{0m} = 0.28$ . Superposed are the best fit parameter values for each one of four truncations of the Gold06p dataset. The best fit parameters for the truncation  $135_{G06p} - 41_{HZSST} - 26_{SCP}$  are shifted by about  $3\sigma$  from corresponding Gold06p best fit values in the direction of  $\Lambda$ CDM.

For example, the  $135_{G06p} - 41_{HZSST} - 26_{SCP}$  truncation shifts the best fit parameter values of the Gold06p by about  $3\sigma$  in the direction of  $\Lambda$ CDM (and beyond it) while the shift with respect to the random truncations of Gold06p is  $3.7\sigma$  (Fig. 5). The corresponding shifts with respect to the Gold06 dataset were about  $1\sigma$  and  $2.6\sigma$  respectively (Figs. 2 and 3).

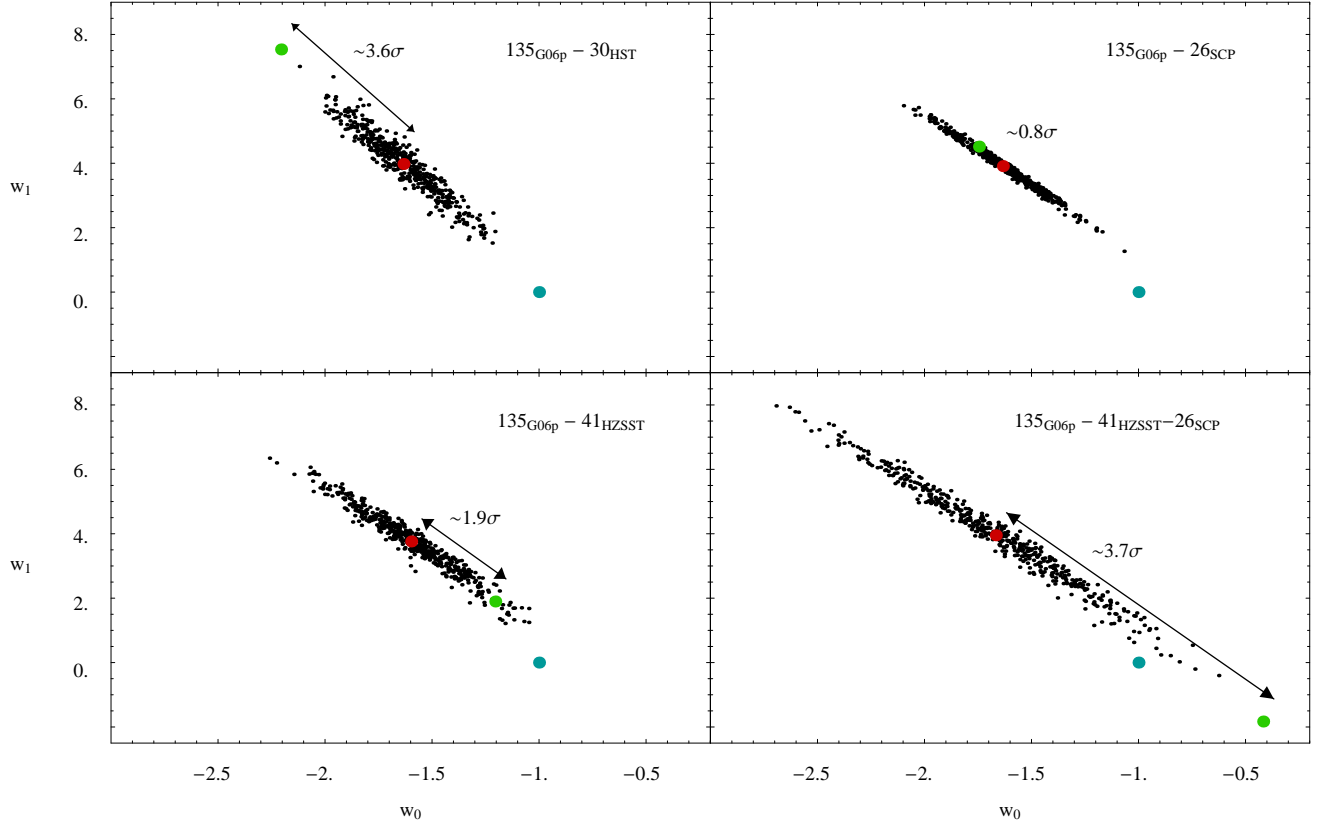


FIG. 5: Comparison of the best fit parameters to the subsample truncations shown in Table III with corresponding random truncations of the Gold06p dataset. In all truncation cases (except of the SCP truncation) the best fit parameter values are shifted (in different directions) by more than  $2\sigma$  from the mean random truncation values. The best fit parameter shift of the  $135_{G06p} - 41_{HZSST} - 26_{SCP}$  is  $3.7\sigma$  compared to the corresponding random truncation. The point corresponding to  $\Lambda$ CDM ( $w_0 = -1, w_1 = 0$ ) is also shown.

### III. DISCUSSION-CONCLUSION

The fact that more recent SnIa data (HST and SNLS) seem to favor  $\Lambda$ CDM significantly more than earlier data (HZSST) makes it possible that earlier data may be more

TABLE III: The four subset truncations of Fig 5.

Dataset	$w_0$	$\frac{w_0^r}{w_1^r}$ (MC)	$\frac{w - \bar{w}^r}{\sigma_{w^r}}$
$135 - 30_{HST}$	$w_0 = -2.21$ $w_1 = 7.53$	$w_0^r = -1.63 \pm 0.17$ $w_1^r = 3.98 \pm 0.97$	$-3.6\sigma$
$135 - 26_{SCP}$	$w_0 = -1.75$ $w_1 = 4.52$	$w_0^r = -1.63 \pm 0.17$ $w_1^r = 3.91 \pm 0.75$	$-0.8\sigma$
$135 - 41_{HZSST}$	$w_0 = -1.20$ $w_1 = 1.90$	$w_0^r = -1.60 \pm 0.21$ $w_1^r = 3.76 \pm 0.95$	$+1.9\sigma$
$135 - 41_{HZSST} - 26_{SCP}$	$w_0 = -0.42$ $w_1 = -1.83$	$w_0^r = -1.67 \pm 0.37$ $w_1^r = 3.95 \pm 1.55$	$+3.7\sigma$

prone to systematic errors. It is therefore interesting to identify a small subset of SnIa from the HZSST data that is mostly responsible for the trend of HZSST towards an evolving  $w(z)$ . We have isolated the group of SnIa in the HZSST subset whose distance modulus differs by more than  $1.8\sigma$  from the  $\Lambda$ CDM predictions ( $\Omega_{0m} = 0.28$ ). The group which consists of just six SnIa is also significantly responsible for the trend of the HZSST subset towards an evolving  $w(z)$ . These SnIa are: (SN99Q2, SN00ee, SN00ec, SN99S, SN01fo, SN99fv). The shifted best fit parameter values ( $w_0, w_1$ ) due to these six SnIa data truncation are shown in Fig. 6a superposed on a Monte-Carlo simulation of corresponding random 6 point truncations to the HZSST subset. We anticipate that the possible systematic errors that lead to the distinct behavior of the HZSST subset are maximal for these six SnIa and it may be easier to identify them and correct them in this set of six SnIa. Alternatively these 6 SnIa could be discarded from the Gold06 dataset as outliers in an effort to improve its statistical uniformity and bring it to line with the more recent data.

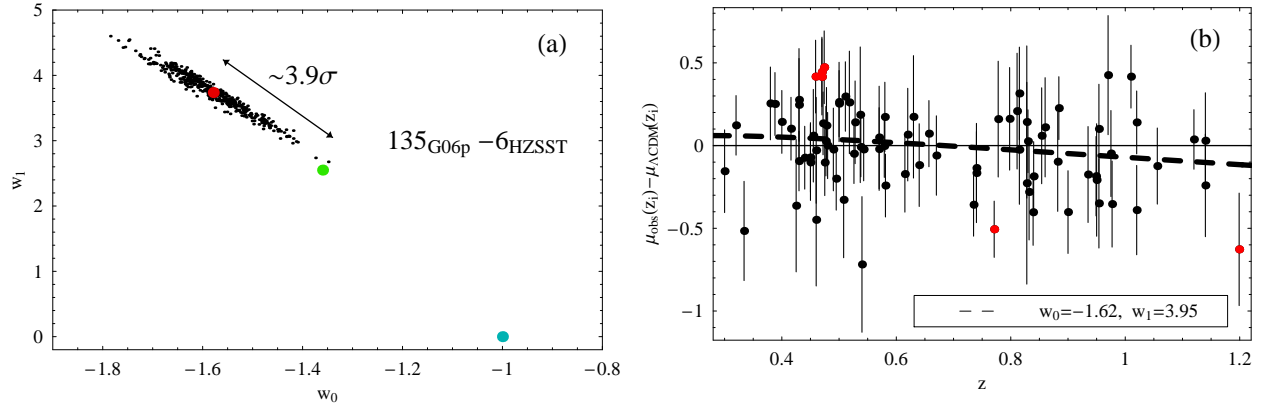


FIG. 6: a. The best fit parameter values for the Gold06p dataset for random 6 point truncations from the HZSST subset. The parameter shift is maximized at  $3.9\sigma$  when the following six points are truncated: (SN99Q2, SN00ee, SN00ec, SN99S, SN01fo, SN99fv) (red dot). These are also the points whose distance modulus differs by more than  $1.8\sigma$  from the  $\Lambda\text{CDM}$  predictions. b. The best fit distance modulus (dashed line) relative to  $\Lambda\text{CDM}$  and the data of the Gold06 dataset in the redshift range of the HZSST subset. The six points of the HZSST subset which differ from  $\Lambda\text{CDM}$  by more than  $1.8\sigma$  are colored in red. They are also the most favorable points for an evolving  $w(z)$ .

A visual display of the six datapoints (points in red) compared to other datapoints is shown in Fig. 6b where we show the distance modulus relative to  $\Lambda\text{CDM}$  ( $\Omega_{0m} = 0.28$ ) of the Gold06 data in the redshift range of the HZSST subset. In the same plot we show (thick dashed line) the distance modulus corresponding to the best fit values ( $w_0 = -1.62, w_1 = 3.95$ ) obtained from the Gold06p data (dashed line) indicating that all of the six red datapoints strongly favor the best fit  $w(z)$  over  $\Lambda\text{CDM}$ .

In conclusion we have demonstrated that despite the careful filtering and the improved calibration, the Gold06 dataset is plagued with statistical inhomogeneities which are possibly due to systematic errors. Given the fact that the more recent data (SNLS and HST) are statistically consistent with each other and homogeneous, it is highly

probable that the possible source of systematic errors lies within the earlier data and in particular in the HZSST subset.

**Numerical Analysis:** The mathematica files and the datafile used in the numerical analysis of this work may be found at <http://leandros.physics.uoi.gr/gold06/gold06.htm>.

### Acknowledgements

This work was supported by the European Research and Training Network MRTPN-CT-2006 035863-1 (UniverseNet). SN acknowledges support from the Greek State Scholarships Foundation (I.K.Y.).

- 
- [1] D. N. Spergel *et al.* [WMAP Collaboration], *Astrophys. J. Suppl.* **148**, 175 (2003).  
[2] M. Tegmark *et al.* [SDSS Collaboration], *Phys. Rev. D* **69**, 103501 (2004).  
[3] Riess et al. 1998 *AJ*, 116, 1009; Clocchiatti et al. 2003, astro-ph/0310432; Riess et al. 2000, *ApJ*, 536, 62; Tonry et al. 2003, *Astrophys.J*594:1-24,2003;  
[4] Perlmutter et al. 1999, *ApJ*, 517, 565;  
[5] Hamuy et al. 1996, *AJ*, 112, 2408; Riess et al. 1999, *AJ*, 117, 707; Jha 2002 (PhD thesis Harvard); Krisciunas 2001, *AJ*, 122, 1616;  
[6] S. Perlmutter et. al., *Nature (London)* **391**, 51(1998); Barris, B *et al.*, 2004 *Astroph. J.* **602** 571; Knop R *et al.*, 2003 *Astroph. J.* **598** 102;  
[7] P. Astier *et al.*, arXiv:astro-ph/0510447.  
[8] A. G. Riess *et al.* [Supernova Search Team Collabora-  
tion], *Astrophys. J.* **607**, 665 (2004).  
[9] A. G. Riess *et al.*, arXiv:astro-ph/0611572.  
[10] T. Padmanabhan, arXiv:gr-qc/0609012.  
[11] E. J. Copeland, M. Sami and S. Tsujikawa, arXiv:hep-th/0603057.  
[12] L. Perivolaropoulos, AIP Conf. Proc. **848**, 698 (2006) [arXiv:astro-ph/0601014].  
[13] J. S. Alcaniz, *Braz. J. Phys.* **36**, 1109 (2006) [arXiv:astro-ph/0608631].  
[14] V. Sahni and A. Starobinsky, arXiv:astro-ph/0610026.  
[15] J. P. Uzan, arXiv:astro-ph/0605313.  
[16] D. Polarski, AIP Conf. Proc. **861**, 1013 (2006) [arXiv:astro-ph/0605532].  
[17] V. Sahni and A. A. Starobinsky, *Int. J. Mod. Phys. D* **9**, 373 (2000) [arXiv:astro-ph/9904398]; S. M. Carroll, *Living Rev. Rel.* **4**, 1 (2001) [arXiv:astro-ph/0004075];

- P. J. E. Peebles and B. Ratra, Rev. Mod. Phys. **75**, 559 (2003) [arXiv:astro-ph/0207347]; T. Padmanabhan, Phys. Rept. **380**, 235 (2003) [arXiv:hep-th/0212290].
- [18] B. Ratra and P.J.E. Peebles, Phys. Rev. D**37**, 3406 (1988); Rev. Mod. Phys. **75**, 559 (2003) [arXiv:astro-ph/0207347]; C. Wetterich, Nucl. Phys. B **302**, 668(1988); P.G.Ferreira and M. Joyce, Phys. Rev. D**58**,023503(1998);M. Sahlen, A. R. Liddle and D. Parkinson, arXiv:astro-ph/0610812.
- [19] B. Boisseau, G. Esposito-Farese, D. Polarski and A. A. Starobinsky, Phys. Rev. Lett. **85**, 2236 (2000)[arXiv:gr-qc/0001066]; F. Perrotta, C. Baccigalupi and S. Matarrese, Phys. Rev. D **61**, 023507 (2000) [arXiv:astro-ph/9906066]; N. Bartolo and M. Pietroni, Phys. Rev. D **61**, 023518 (2000) [arXiv:hep-ph/9908521]; L. Perivolaropoulos, arXiv:astro-ph/0504582, **JCAP** **10**, 001 (2005); L. Perivolaropoulos, Phys. Rev. D **67**, 123516 (2003) [arXiv:hep-ph/0301237]; D.F.Torres, Phys. Rev. D**66**,043522(2002); L. Perivolaropoulos and C. Sourdis,Phys. Rev. D **66**, 084018 (2002) [arXiv:hep-ph/0204155]; L. Amendola, Phys. Rev. D **62**, 043511 (2000) [arXiv:astro-ph/9908023].
- [20] S. Nojiri and S. D. Odintsov, arXiv:hep-th/0601213.
- [21] L. Amendola, D. Polarski and S. Tsujikawa, arXiv:astro-ph/0603703.
- [22] T. Chiba, Phys. Lett. B **575**, 1 (2003) [arXiv:astro-ph/0307338].
- [23] S. Nojiri and S. D. Odintsov, Phys. Rev. D **68**, 123512 (2003) [arXiv:hep-th/0307288].
- [24] S. Nojiri and S. D. Odintsov, arXiv:hep-th/0611071.
- [25] I. Y. Aref'eva, A. S. Koshelev and S. Y. Vernov, Phys. Rev. D **72**, 064017 (2005) [arXiv:astro-ph/0507067].
- [26] R. Lazkoz, R. Maartens and E. Majerotto, Phys. Rev. D **74**, 083510 (2006) [arXiv:astro-ph/0605701].
- [27] C. Bogdanos, A. Dimitriadis and K. Tamvakis, arXiv:hep-th/0611181.
- [28] R. G. Cai, Y. g. Gong and B. Wang, **JCAP** **0603**, 006 (2006) [arXiv:hep-th/0511301].
- [29] S. Nojiri, S. D. Odintsov and M. Sasaki, Phys. Rev. D **71**, 123509 (2005) [arXiv:hep-th/0504052].
- [30] T. D. Saini, S. Raychaudhury, V. Sahni and A. A. Starobinsky, Phys. Rev. Lett. **85**, 1162 (2000) [arXiv:astro-ph/9910231].
- [31] S. Nesseris and L. Perivolaropoulos, Phys. Rev. D **70**, 043531 (2004) [arXiv:astro-ph/0401556].
- [32] D. Huterer and M. S. Turner, Phys. Rev. D **64**, 123527 (2001) [arXiv:astro-ph/0012510].
- [33] <http://www.tass-survey.org/richmond/sne/sn.list>;
- [34] M. Chevallier and D. Polarski, Int. J. Mod. Phys. D **10**, 213 (2001) [arXiv:gr-qc/0009008].
- [35] E. V. Linder, Phys. Rev. Lett. **90**, 091301 (2003) [arXiv:astro-ph/0208512].
- [36] R. Lazkoz, S. Nesseris and L. Perivolaropoulos, **JCAP** **0511**, 010 (2005) [arXiv:astro-ph/0503230].
- [37] S. Nesseris and L. Perivolaropoulos, Phys. Rev. D **72**, 123519 (2005) [arXiv:astro-ph/0511040].
- [38] H. K. Jassal, J. S. Bagla and T. Padmanabhan, Phys. Rev. D **72**, 103503 (2005) [arXiv:astro-ph/0506748].
- [39] U. Alam, V. Sahni and A. A. Starobinsky, **JCAP** **0406**, 008 (2004) [arXiv:astro-ph/0403687].
- [40] Y. Wang and P. Mukherjee, Astrophys. J. **650**, 1 (2006) [arXiv:astro-ph/0604051].
- [41] R. A. Daly and S. G. Djorgovski, arXiv:astro-ph/0609791.
- [42] D. Huterer and A. Cooray, Phys. Rev. D **71**, 023506 (2005) [arXiv:astro-ph/0404062].
- [43] A. Shafieloo, U. Alam, V. Sahni and A. A. Starobinsky, Mon. Not. Roy. Astron. Soc. **366**, 1081 (2006) [arXiv:astro-ph/0505329].
- [44] R. Gannouji, D. Polarski, A. Ranquet and A. A. Starobinsky, **JCAP** **0609**, 016 (2006) [arXiv:astro-ph/0606287].
- [45] Z. K. Guo, Y. S. Piao, X. Zhang and Y. Z. Zhang, arXiv:astro-ph/0608165.
- [46] J. Kujat, R. J. Scherrer and A. A. Sen, Phys. Rev. D **74**, 083501 (2006) [arXiv:astro-ph/0606735].
- [47] H. S. Zhang and Z. H. Zhu, arXiv:astro-ph/0611834.
- [48] S. Nesseris and L. Perivolaropoulos, arXiv:astro-ph/0611238.
- [49] F. Bricscese, E. Elizalde, S. Nojiri and S. D. Odintsov, arXiv:hep-th/0612220.
- [50] E. O. Kahya and V. K. Onemli, arXiv:gr-qc/0612026.
- [51] B. McInnes, Nucl. Phys. B **718**, 55 (2005) [arXiv:hep-th/0502209].
- [52] U. Alam, V. Sahni and A. A. Starobinsky, arXiv:astro-ph/0612381.
- [53] Y. G. Gong and A. z. Wang, arXiv:astro-ph/0612196.

#### IV. APPENDIX

TABLE IV: The Gold06 dataset with its subsets. The

<b>SN</b>	<b><math>z</math></b>	$\mu_0$	$\sigma_{\mu_0}$	<b>Subsample</b>
SN03D1au	0.504	42.61	0.17	SNLS
SN03D1aw	0.582	43.07	0.17	SNLS
SN03D1ax	0.496	42.36	0.17	SNLS
SN03D1cm	0.870	44.28	0.34	SNLS
SN03D1co	0.679	43.58	0.19	SNLS
SN03D1fc	0.331	41.13	0.17	SNLS
SN03D1fl	0.688	43.23	0.17	SNLS
SN03D1fq	0.800	43.67	0.19	SNLS
SN03D3af	0.532	42.78	0.18	SNLS
SN03D3aw	0.449	42.05	0.17	SNLS
SN03D3ay	0.371	41.67	0.17	SNLS
SN03D3bh	0.249	40.76	0.17	SNLS
SN03D3cc	0.463	42.27	0.17	SNLS
SN03D3cd	0.461	42.22	0.17	SNLS
SN03D4ag	0.285	40.92	0.17	SNLS
SN03D4at	0.633	43.32	0.18	SNLS
SN03D4cx	0.949	43.69	0.32	SNLS
SN03D4cz	0.695	43.21	0.19	SNLS
SN03D4dh	0.627	42.93	0.17	SNLS
SN03D4di	0.905	43.89	0.30	SNLS
SN03D4dy	0.604	42.70	0.17	SNLS
SN03D4fd	0.791	43.54	0.18	SNLS
SN03D4gg	0.592	42.75	0.19	SNLS
SN03D4gl	0.571	42.65	0.18	SNLS
SN04D1ag	0.557	42.70	0.17	SNLS
SN04D2cf	0.369	41.67	0.17	SNLS
SN04D2fp	0.415	41.96	0.17	SNLS
SN04D2fs	0.357	41.63	0.17	SNLS
SN04D2gb	0.430	41.96	0.17	SNLS
SN04D2gp	0.707	43.42	0.21	SNLS
SN04D3co	0.620	43.21	0.18	SNLS
SN04D3cy	0.643	43.21	0.18	SNLS
SN04D3df	0.470	42.45	0.17	SNLS
SN04D3do	0.610	42.98	0.17	SNLS
SN04D3ez	0.263	40.87	0.17	SNLS
SN04D3fk	0.358	41.66	0.17	SNLS
SN04D3fq	0.730	43.47	0.18	SNLS
SN04D3hn	0.552	42.65	0.17	SNLS
SN04D3kr	0.337	41.44	0.17	SNLS
SN04D3lu	0.822	43.73	0.27	SNLS
SN04D3ml	0.950	44.14	0.31	SNLS
SN04D3nh	0.340	41.51	0.17	SNLS
SN04D3oe	0.756	43.64	0.17	SNLS
SN04D4an	0.613	43.15	0.18	SNLS
SN04D4bq	0.550	42.67	0.17	SNLS
SN04D4dm	0.811	44.13	0.31	SNLS
SN04D4dw	0.961	44.18	0.33	SNLS
1997ff	1.755	45.35	0.35	HST
2002dc	0.475	42.24	0.20	HST
2002dd	0.950	43.98	0.34	HST
2003eq	0.840	43.67	0.21	HST
2003es	0.954	44.30	0.27	HST
2003eb	0.900	43.64	0.25	HST

six outliers of the HZSST subset are denoted by a \*.

<b>SN</b>	<b><math>z</math></b>	$\mu_0$	$\sigma_{\mu_0}$	<b>Subsample</b>
2003XX	0.935	43.97	0.29	HST
2003bd	0.670	43.19	0.24	HST
2002kd	0.735	43.14	0.19	HST
2003be	0.640	43.01	0.25	HST
2003dy	1.340	44.92	0.31	HST
2002ki	1.140	44.71	0.29	HST
2002hp	1.305	44.51	0.30	HST
2002fw	1.300	45.06	0.20	HST
HST04Pat	0.970	44.67	0.36	HST
HST04Mcg	1.370	45.23	0.25	HST
HST05Fer	1.020	43.99	0.27	HST
HST05Koe	1.230	45.17	0.23	HST
HST04Gre	1.140	44.44	0.31	HST
HST04Omb	0.975	44.21	0.26	HST
HST05Lan	1.230	44.97	0.20	HST
HST04Tha	0.954	43.85	0.27	HST
HST04Rak	0.740	43.38	0.22	HST
HST04Yow	0.460	42.23	0.32	HST
HST04Man	0.854	43.96	0.29	HST
HST05Spo	0.839	43.45	0.20	HST
HST04Eag	1.020	44.52	0.19	HST
HST05Gab	1.120	44.67	0.18	HST
HST05Str	1.010	44.77	0.19	HST
HST04Sas	1.390	44.90	0.19	HST
SN95K	0.478	42.48	0.23	HZSST
SN96E	0.425	41.69	0.40	HZSST
SN96H	0.620	43.11	0.28	HZSST
SN96I	0.570	42.80	0.25	HZSST
SN96J	0.300	41.01	0.25	HZSST
SN96K	0.380	42.02	0.22	HZSST
SN96U	0.430	42.33	0.34	HZSST
SN97as	0.508	42.19	0.35	HZSST
SN97bb	0.518	42.83	0.31	HZSST
SN97bj	0.334	40.92	0.30	HZSST
SN97ce	0.440	42.07	0.19	HZSST
SN97cj	0.500	42.73	0.20	HZSST
SN98ac	0.460	41.81	0.40	HZSST
SN98M	0.630	43.26	0.37	HZSST
SN98J	0.828	43.59	0.61	HZSST
SN99Q2*	0.459	42.67	0.22	HZSST
SN99U2	0.511	42.83	0.21	HZSST
SN99S*	0.474	42.81	0.22	HZSST
SN99N	0.537	42.85	0.41	HZSST
SN99fn	0.477	42.38	0.21	HZSST
SN99ff	0.455	42.29	0.28	HZSST
SN99fj	0.815	43.75	0.33	HZSST
SN99fm	0.949	44.00	0.24	HZSST
SN99fk	1.056	44.35	0.23	HZSST
SN99fw	0.278	41.01	0.41	HZSST
SN99fv*	1.199	44.19	0.34	HZSST
SN00ec*	0.470	42.76	0.21	HZSST
SN00dz	0.500	42.74	0.24	HZSST
SN00eg	0.540	41.96	0.41	HZSST

TABLE IV continued

<b>SN</b>	<i>z</i>	$\mu_0$	$\sigma_{\mu_0}$	<b>Subsample</b>
SN00ee*	0.470	42.73	0.23	HZSST
SN00eh	0.490	42.40	0.25	HZSST
SN01jh	0.884	44.22	0.19	HZSST
SN01hu	0.882	43.89	0.30	HZSST
SN01iy	0.570	42.87	0.31	HZSST
SN01jp	0.528	42.76	0.25	HZSST
SN01fo*	0.771	43.12	0.17	HZSST
SN01hs	0.832	43.55	0.29	HZSST
SN01hx	0.798	43.88	0.31	HZSST
SN01hy	0.811	43.97	0.35	HZSST
SN01jf	0.815	44.09	0.28	HZSST
SN01jm	0.977	43.91	0.26	HZSST
SN95aw	0.400	42.04	0.19	SCP
SN95ax	0.615	42.85	0.23	SCP
SN95ay	0.480	42.37	0.20	SCP
SN95az	0.450	42.13	0.21	SCP
SN95ba	0.388	42.07	0.19	SCP
SN96ci	0.495	42.25	0.19	SCP
SN96cl	0.828	43.96	0.46	SCP
SN97eq	0.538	42.66	0.18	SCP
SN97ek	0.860	44.03	0.30	SCP
SN97ez	0.778	43.81	0.35	SCP
SN97F	0.580	43.04	0.21	SCP
SN97H	0.526	42.56	0.18	SCP
SN97I	0.172	39.79	0.18	SCP
SN97N	0.180	39.98	0.18	SCP
SN97P	0.472	42.46	0.19	SCP
SN97Q	0.430	41.99	0.18	SCP
SN97R	0.657	43.27	0.20	SCP
SN97ac	0.320	41.45	0.18	SCP
SN97af	0.579	42.86	0.19	SCP
SN97ai	0.450	42.10	0.23	SCP
SN97aj	0.581	42.63	0.19	SCP
SN97am	0.416	42.10	0.19	SCP
SN97ap	0.830	43.85	0.19	SCP
SN98ba	0.430	42.36	0.25	SCP
SN98bi	0.740	43.35	0.30	SCP
SN00fr	0.543	42.67	0.19	SCP

TABLE IV continued

<b>SN</b>	<i>z</i>	$\mu_0$	$\sigma_{\mu_0}$	<b>Subsample</b>
SN92bs	0.063	37.67	0.19	LR
SN94M	0.024	35.09	0.22	LR
SN94T	0.036	36.01	0.21	LR
SN97dg	0.029	36.13	0.21	LR
SN00bk	0.026	35.35	0.23	LR
SN98cs	0.032	36.08	0.20	LR
SN00cf	0.036	36.39	0.19	LR
SN98dx	0.053	36.95	0.19	LR
SN99gp	0.026	35.57	0.21	LR
SN99X	0.025	35.40	0.22	LR
SN99cc	0.031	35.84	0.21	LR
SN94Q	0.029	35.70	0.21	LR
SN95ac	0.049	36.55	0.20	LR
SN96bl	0.034	36.19	0.20	LR
SN90O	0.030	35.90	0.21	LR
SN96C	0.027	35.90	0.21	LR
SN96ab	0.124	39.19	0.22	LR
SN99ef	0.038	36.67	0.19	LR
SN92J	0.046	36.35	0.21	LR
SN92bk	0.058	37.13	0.19	LR
SN92bp	0.079	37.94	0.18	LR
SN92br	0.088	38.07	0.28	LR
SN93H	0.025	35.09	0.22	LR
SN93ah	0.028	35.53	0.22	LR
SN90T	0.040	36.38	0.20	LR
SN90af	0.050	36.84	0.22	LR
SN91U	0.033	35.53	0.21	LR
SN91S	0.056	37.31	0.19	LR
SN92P	0.026	35.63	0.22	LR
SN92bg	0.036	36.17	0.20	LR
SN92bl	0.043	36.52	0.19	LR
SN92bh	0.045	36.99	0.18	LR
SN92au	0.061	37.31	0.22	LR
SN92ae	0.075	37.77	0.19	LR
SN92aq	0.101	38.70	0.20	LR
SN93ag	0.050	37.07	0.19	LR
SN93O	0.052	37.16	0.18	LR
SN93B	0.071	37.78	0.19	LR